Measuring the roughness of buried interfaces by sputter depth profiling

2013 Nanotechnology 24 015708

(http://iopscience.iop.org/0957-4484/24/1/015708)

Nanotechnology **24** (2013) 015708 (6pp) doi:10.1088/0957-4484/24/1/015708

Measuring the roughness of buried interfaces by sputter depth profiling

S V Baryshev[1], J A Klug[1], A V Zinovev[1], C E Tripa[1], Q Peng[2,3], J W Elam[2] and I V Veryovkin[1]

[1] Materials Science Division, Argonne National Laboratory, 9700 S. Cass Ave., Argonne, IL 60439, USA
[2] Energy Systems Division, Argonne National Laboratory, 9700 S. Cass Ave., Argonne, IL 60439, USA

E-mail: sergey.v.baryshev@gmail.com and sbaryshev@anl.gov

Received 30 June 2012, in final form 14 November 2012
Published 7 December 2012
Online at stacks.iop.org/Nano/24/015708

Abstract
We report results of high-resolution sputter depth profiling of an alternating MgO/ZnO nanolayer stack grown by atomic layer deposition (ALD) of ≈5.5 nm per layer. We used an improved dual beam time-of-flight secondary ion mass spectrometer to measure $^{24}Mg^+$ and $^{64}Zn^+$ intensities as a function of sample depth. Analysis of depth profiles by the mixing–roughness–information model yields a 1.5 nm nanolayer interfacial roughness within the MgO/ZnO multilayer. This finding was cross-validated using specular x-ray reflectivity. Such an analysis further suggested that the 1.5 nm roughness corresponds to native/jig-sawed interfacial roughness rather than interfacial interdiffusion during the ALD growth.

(Some figures may appear in colour only in the online journal)

1. Introduction

The roughness of interfaces in multilayered materials is of great interest and extreme importance. This parameter strongly impacts basic materials properties, such as heat transfer [1], electron transport [2] and magnetism [3], and device performance in a wide range of technologies including spin-based electronics [4], giant magnetoresistance structures/devices [5], high-*k* multilayer materials [6], artificial Bragg crystals [7] and resistive random access memory [8].

Three important parameters for characterizing multilayered materials are (i) the single layer thickness, (ii) the interfacial roughness and (iii) the density. A powerful and efficient method to determine their values combines x-ray reflectivity (XRR) with ellipsometry. Both techniques are nondestructive, and they do not require sample preparation. XRR uses the values of (i), (ii) and (iii) as fitting parameters jointly with some types of boundary conditions to solve a general inverse wave scattering problem [9, 10]. Ellipsometry relies on the refractive index (a function of density) and layer thicknesses, and depends on the boundary conditions as well. This makes the data fitting model-sensitive and dependent on many free parameters, which can become intractable as the number of layers in the layered structure increases. Moreover, such indirect techniques may become inefficient for samples where the repetition of certain layers in an *n*-layer stack varies, as, for instance, occurs in the case of metamaterials [11, 12]. A problem will also exist for multilayer semiconductor heterostructures, where the compositional variation between adjacent layers that differ by only a few per cent in solid solution content [13] provides insufficient density contrast for characterization by XRR, and refractive index changes that are too small for ellipsometry to be accurate. Importantly, XRR cannot distinguish between the interfacial roughness and the interdiffusion for buried interfaces [10].

Another widely used approach for direct evaluation of buried interfaces, transmission electron microscopy (TEM), lacks some of XRR's advantages. The TEM sample preparation procedure is destructive and can cause undesirable side effects (e.g., from the 30 keV focused Ga^+ ion beam used to cut cross sections of interfaces) that can complicate the interpretation of final results. TEM images typically represent cross sections within a small field of view (≤50 nm). To be precise and quantitative, it requires cumbersome and/or indirect image processing [14], which becomes ambiguous when the layer thickness approaches 5 nm or less [15].

[3] Current address: Electrical and Computer Engineering Department, Duke University, 100 Science Drive, Durham, NC 27708, USA.

Thus, a more direct technique for characterization of nm-thick layers in multilayered structures is highly desirable. It should be independent of optical properties and rely on simpler and more straightforward data post-processing, and it should be either nondestructive or not require sample preparation, or both. Such a technique could complement the established XRR, ellipsometry and TEM methods by providing additional insight into the sample structure through the specified advantages.

Mass spectrometry is vital in basic physics [16], chemistry [17] and materials science [18] due to a number of unique advantages, such as sensitivity to isotopic ratio, trace amounts of elemental/molecular species on the surface and in the bulk, etc. In this context, an extension of its capabilities is of great interest. In this paper, we demonstrate that properly designed mass spectrometry of secondary ion species in sputter depth profiling experiments can successfully reveal structural features of multi-nanolayered materials and characterize their surfaces and interfaces. To this end, improved dual beam secondary ion mass spectrometry (SIMS) with low energy normal incidence milling was applied to depth profile a nanolayered |MgO/ZnO| × 8 structure grown by atomic layer deposition (ALD). The resulting depth profiles were processed using a mixing–roughness–information (MRI) model. This model has analytical solutions with, in the case of SIMS, two variable parameters having straightforward physical interpretations: the ion beam mixing length and the roughness. The SIMS-MRI results were compared to structural parameters obtained by XRR measurements to confirm the validity of the conclusions.

2. Experimental details

A layered structure comprised of |5.5 nm MgO/5.5 nm ZnO| × 8 was grown by ALD on a polished Si(100) substrate at 200 °C using established precursor chemistries for MgO [19] and ZnO [20, 21]. The precursor vapors were transported through heated lines into the reactor by a 360 sccm (standard cubic centimeter per minute) ultrahigh purity N_2 flow at a pressure of 1 Torr. The 5.5 nm ZnO layers were deposited using 32 cycles of alternating exposures to diethyl zinc, $(C_2H_5)_2Zn$, and distilled H_2O. The 5.5 nm MgO layers were prepared using 39 cycles of alternating exposures to bis(cyclopentadienyl)magnesium(II), $(C_5H_5)_2Mg$, and distilled H_2O. The final layered structure consisted of eight pairs of MgO/ZnO with the ZnO layer applied first to the Si(100) wafer. The MgO and ZnO growth rates were 1.4 and 1.7 Å per cycle, respectively, as determined using spectroscopic ellipsometry. The multilayer was characterized by x-ray diffraction and ellipsometry. The structural data obtained from these measurements indicated that the MgO layers were amorphous and the ZnO layers were polycrystalline in the wurtzite phase. The roughness of the Si substrate was ≈0.3 nm. The layer-to-layer mixing due to thermal diffusion during ALD performed at $T = 200$ °C is expected to be low.

Specular x-ray reflectivity (XRR) measurements were made with a Philips X'Pert Pro MRD diffractometer using Cu Kα radiation ($\lambda = 1.5418$ Å) and operating at 30 kV/40 mA. The incident x-ray beam was conditioned by a 60 mm graded parabolic W/Si mirror with a 0.8° acceptance angle and a 1/32° divergence slit. The reflected beam was collected with a PW3011/20 sealed proportional point detector positioned behind a 0.27° parallel plate collimator.

Secondary ion mass spectrometry studies were performed in a custom-designed SARISA (surface analysis by resonance ionization of sputtered atoms) instrument in the Materials Science Division at Argonne National Laboratory [22]. SARISA combines two independently optimized Ar^+ ion beams: one of low energy (a few hundred eV) and normal incidence for ultimate depth resolution ion milling/sputtering, and another for elemental time-of-flight (TOF) SIMS analysis with high lateral resolution. This arrangement is based on the known powerful dual beam approach to depth profiling [23] and can be dubbed *gentle*DB[4]. There are three main advantages of this setup. First, depth resolution is controlled by the milling normally incident beam if the parameter α (defined in the next paragraph) is much smaller than unity, or $\alpha \ll 1$. Second and third, normal incidence permits variation of the impact energy of the primary ions by target bias and does not introduce additional roughening of the sample surface [24, 25].

Elemental depth profiles, concentration/intensity versus depth, of the sandwich structure were obtained by a sequence of alternating cycles. Ion milling by a raster scanned primary direct current (dc) Ar^+ ion beam at 500 eV and normal incidence was followed by TOF SIMS analysis of the revealed subsurface by a raster scanned pulsed (200 ns long) Ar^+ ion beam at 5 keV energy and 60° incidence with respect to the target normal, as shown schematically in figure 1(a). This pair of cycles was repeated multiple times until the Si substrate was reached, which was monitored by the Si^+ peak intensity in the mass spectrum. In the depth profile, the Si substrate grew in as a spike attributed to the ∼100-fold enhanced secondary ion yield due to the presence of native SiO_2 on the Si substrate surface. The Si^+ peak intensity then stabilized at a lower constant level, as shown in figure 1(b). It is important to understand that both beams in the *gentle*DB arrangement sputter/destroy the material: the orthogonal milling beam to dig through the sample, and the analysis/probing one to produce secondary ions to be analyzed. The depth resolution is controlled ultimately by the milling beam characteristics. This condition is fulfilled if the effective erosion efficiency, $E = Yjt/e$, of the milling beam is much higher than that of the analytical beam, or $\alpha = E_{\text{analysis}}/E_{\text{milling}} \ll 1$. Here, Y is the sputtering yield, which depends on the beam energy ε, the primary projectile species and the incident angle, j is the current density and t is the total sputtering time during which the ion beam is on. In our experimental setup, $\alpha \sim 10^{-5}$.

The milling beam was digitally raster scanned over a square region with an area of ≈1 mm^2 (blue square in figure 1(a)), while the analytical beam was raster scanned over a square of ≈500 × 500 μm^2 (green square in figure 1(a)).

[4] It is dubbed *gentle*DB because of the capability of the low energy normally incident milling to *gently*, layer by layer, remove sample material.

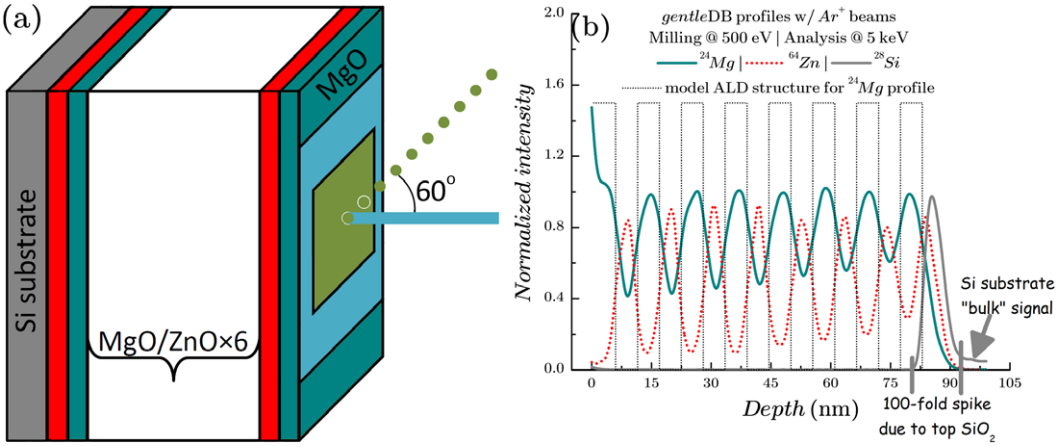

Figure 1. (a) Simplified experimental setup: 8 MgO (cyan)/ZnO (red) pairs. The superimposed and centered blue and green squares are (i) a crater from the raster scanned direct current normal incidence milling Ar^+ beam (impinging solid blue line), and (ii) a raster-scan area from the pulsed probing Ar^+ beam (impinging green dotted line), respectively. (b) Full *gentle*DB TOF SIMS depth profiles of the MgO/ZnO × 8 ALD structure on the Si substrate obtained by the orthogonal 500 eV milling Ar^+ beam combined with the 60° 5 keV probing Ar^+ beam.

Both raster areas were precisely overlapped using an *in situ* Schwarzschild microscope [22], and *ex situ* using white light profilometry [26].

The ion beam currents were measured and focused *in situ* by a custom graphite Faraday cup (FC) consisting of an internal pin (inlet holes of 250 μm diameter) and the external surface. This design provides control over the ion beam focusing conditions. The ion beam profiles were found to have a symmetric Gaussian-like distribution by burning dents in soft materials and profiling the dents by *ex situ* white light profilometry [26]. The well-defined beam profile allows one to precisely calculate the ion beam current density using the dc current value measured on the FC. The milling beam parameters at 500 eV were 1 μA dc and a full width at half-maximum (FWHM) of ≈150 μm. The analytical beam characteristics at 5 keV were 300 nA dc and an FWHM of ≈40 μm, and then reduced down to 30 nA by choosing an appropriate aperture. The measured energy spread, $\Delta\varepsilon$, of our low energy column [22] was 23 eV, yielding $\Delta\varepsilon/\varepsilon \approx 5\times10^{-2}$ at 500 eV milling energy. Thus, the milling beam could be considered as monoenergetic.

3. Results, discussion and conclusion

Figure 1(b) demonstrates the SIMS depth profiles of Mg^+ and Zn^+ obtained by *gentle*DB at 500 eV ion milling, reflecting the full set of eight peaks for MgO and ZnO in the periodical structure where the spacing between consecutive data points is ≈0.8 nm. Figure 2(a) is a high-resolution profile obtained under the same conditions as the profiles in figure 1(b), but using smaller ion milling increments, so that the depth difference between two consecutive points is ≈0.2 nm, corresponding to the monolayer thickness for wurtzite ZnO.

We used the high-resolution Zn^+ depth profile (measured in great detail) in figure 2(a) to evaluate the structure of the ALD multilayer stack by means of the mixing–roughness–information (MRI) model (see the appendix for more details) [27, 28]. In essence, this model has three physically meaningful parameters. The mixing is characterized by the ion beam mixing length, w. This parameter describes how two dissimilar layers with a perfectly abrupt interface experience mutually uniform interpenetration under nonreactive gas bombardment. The roughness is the root-mean-square (RMS) roughness, σ. The 'information depth', λ, is equivalent to the escape depth commonly used in surface analysis. In general, λ is a variable parameter, but in the case of SIMS it can be fixed at a value of 1–2 monolayers [29]. The effects of the two main processes, mixing and roughness, on the resulting peak depth profile are shown in figure 2(b). In the case of an ideal rectangular layer, the ion beam induced mixing leads to an asymmetric depth profile. The roughness may broaden and symmetrize the profile depending on the interplay between the w and σ values. The effect of the information depth λ is not incorporated, since it is expected to be negligible.

The dark gray solid curve in figure 2(a) superimposed on the Zn^+ depth profile is the best fit of the experimental curve by the MRI model. The fit parameters were as follows: w = 0.4 nm, σ = 1.5 nm, and λ was fixed at 0.2 nm, corresponding to the wurtzite ZnO monolayer thickness. The flat thickness, d, which is the thickness of an ideal flat layer (see figure 2(b)) that defines the boundary conditions for the model, appeared to be 3 nm, yielding a total thickness of 6 nm ($=d + 2\sigma$). The sharpness of the interface between the Si substrate and the final ZnO layer can also be estimated. The up-slope of the Si signal in figure 1(b) implies a roughness of ≈0.4 nm.

To cross-validate the results obtained by MRI modeling of the experimental data, we performed specular XRR measurements on a MgO/ZnO sample prepared under identical conditions. Figure 3 represents a typical specular XRR profile obtained for the ALD multilayer sample. The data were fitted using a commercial software package (Panalytical X'Pert Reflectivity) which makes use of the Parratt recursion formalism for reflectivity [30]. Due to the relatively large number of discrete layers present in the

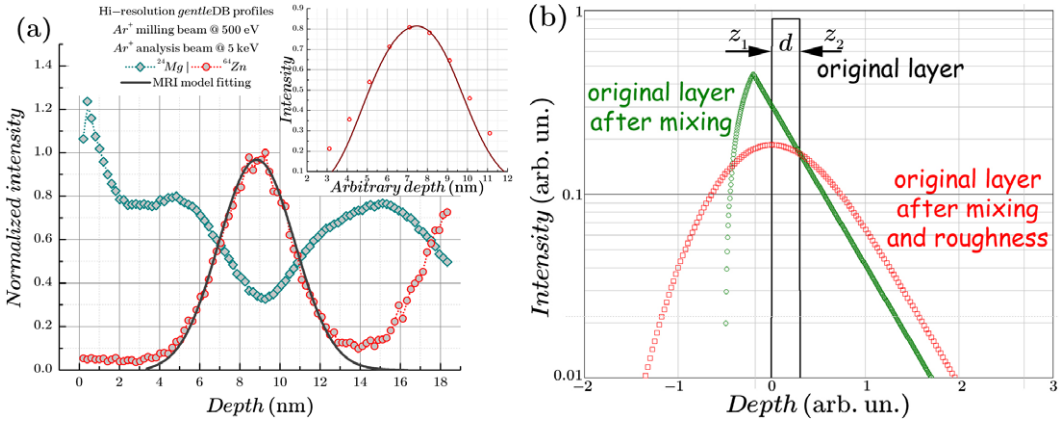

Figure 2. (a) High-resolution *gentle*DB TOF SIMS depth profiles of MgO/ZnO top layers obtained by the 500 eV milling Ar^+ beam and the 5 keV analysis Ar^+ beam. The Mg^+ signal is shown in cyan (open diamonds) and the Zn^+ signal is shown in red (open circles). The dark gray solid curve is the best MRI model fit. The inset represents the seventh peak taken from figure 1(b): the points show the experimental curve while the wine solid curve is the MRI model fit. (b) Principles of the MRI model describing how different distortion sources affect an ideal, rectangular (flat) layer profile of thickness d. The effect of the escape depth parameter, negligible in the case of SIMS, would slightly broaden the red curve (open squares) and is not shown.

|MgO/ZnO| × 8 heterostructure, several periodic constraints were applied to reduce the set of fitting parameters. A simple periodic model assuming identical ZnO/MgO bilayers failed to reasonably approximate the data. A second model where the first ZnO layer and the last MgO layer were treated discretely, as described by Jensen *et al* [10], also failed to produce adequate fits to the experimental data. However, simulations where the density, ρ, thickness and roughness, σ, of each subsequent ZnO and MgO layer were constrained to increase linearly with increasing distance from the substrate provided a good match to the experimental reflectivity curve. The experimental fit was further optimized by allowing each ρ, thickness and σ value to vary from the linear model within reasonable physical constraints (e.g. bulk density values). The average values resulting from the optimized fit were a thickness of 6.4 nm and $\sigma = 1.0 \pm 0.2$ nm for the ZnO, and a thickness of 6.1 nm and $\sigma = 1.5 \pm 0.3$ nm for the MgO[5]. These average values determined from the XRR measurements match the values of total thickness of 6 nm and $\sigma = 1.5$ nm extracted from the SIMS analysis very well. In addition, the optimized XRR fit yielded a thickness of 1.2 nm and $\sigma = 0.3$ nm for the native SiO_2 layer on the Si substrate, in good agreement with the value of 0.4 nm measured by SIMS.

Thus, XRR data independently prove that SIMS analysis along with the chemical information is capable of revealing the detailed internal interface structure when the distortions/artifacts related to a profiling procedure are minimized to be much smaller than the features to be investigated. In the case of *gentle*DB, this means that the extracted mixing parameter $w = 0.4$ nm, is of the same order as the inherent escape depth of a secondary ion, the physical limitation of the technique. Therefore, the interfacial roughness of 1.5 nm found for the MgO/ZnO layers is owing

[5] To correctly compare these two mathematic roughness parameters, contained within the Parratt formalism, to the corresponding results of the SIMS-MRI approach, their average value should be calculated, $(1 + 1.5)/2$ nm, yielding $\sigma = 1.3$ nm.

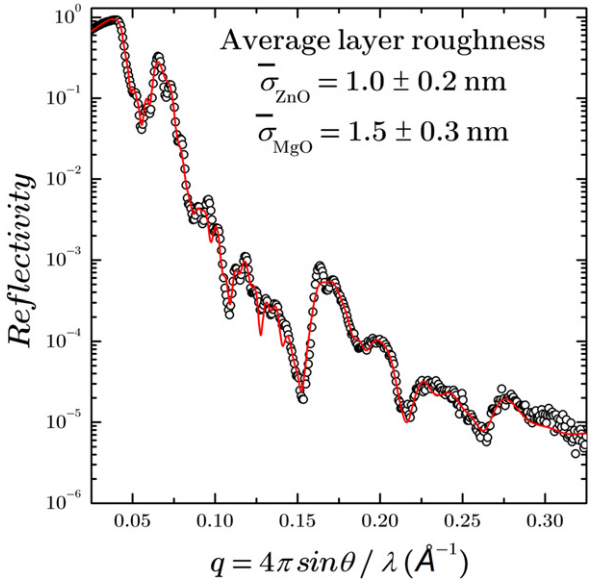

Figure 3. Specular XRR profile of the ALD MgO/ZnO multilayer on the Si substrate obtained with 1.5418 Å irradiation. The black circles show the experimental reflectivity curve, while the simulated reflectivity curve is represented by the red solid line.

to an ultra-short ion beam mixing length/lattice disturbance range, feasible in the *gentle*DB profiling procedure. XRR also proves that the obtained 1.5 nm roughness is reasonable and falls well within the range provided by other experimental methods, both in this study and in other studies of layered nanolaminate oxides performed by AFM/STM [31], XRR [6, 10] and TEM [6, 21].

Let us extend the findings by *gentle*DB SIMS in conjunction with MRI results. As was mentioned above, XRR cannot distinguish between the interfacial roughness and the interdiffusion [10]. One may assume that the interdiffusion at the interface is a process similar in some way to the ion beam mixing, which normally causes a

mutually uniform layer interpenetration [32], thus blurring the initially sharp interfaces and forming a mixed-up interlayer. If the interdiffusion is pronounced, the MRI model suggests that the *gentle*DB SIMS depth profiles would look more asymmetric, closer to the green curve shown in figure 2(b). There are several practical considerations to prove this point. For this particular MgO/ZnO structure grown at 200 °C, the shapes of the measured Mg^+ and Zn^+ depth profile peaks, corresponding to top layers, are broad and nearly symmetric. In the context of the previously described advantages of the low energy orthogonal milling, this suggests that the estimated 1.5 nm roughness corresponds to the native (i.e., 'jig-saw' shaped) interface roughness rather than to interdiffusion, or that the interdiffusion does not exceed 0.4 nm from the total 1.5 nm. At the same time, as is known for ALD multilayers comprised of metal-oxide binaries, the interdiffusion is suppressed, i.e., the diffusion coefficients are low under the reported synthetic conditions. Nevertheless, in figure 1(b) a slight loss of resolution with depth is observed (the valley intensities move up slowly). We believe this is due to the fact that the deeper layers have longer diffusion times during the growth, yet the diffusion coefficients are low (cumulative effect). Hence, the top layers are less affected by the ever-present interdiffusion than the deeper layers. A similar effect was observed for multiple boron δ-layers in silicon [24]. From the XRR data, it is seen that the ZnO layer roughness gradually grows from 0.5 nm (at the substrate) to 1.4 nm for the top layer (yielding an average σ of 1 nm, as reported in figure 3). If the MRI fitting of the seventh Zn^+ peak is performed, it provides $d = 5$ nm, $\sigma = 0.8$ nm and $w = 1$ nm (the inset in figure 2(a)), compared to XRR's thickness of 5.4 nm and σ of 0.6 nm. In this case, the shape of the Zn profile is slightly asymmetric, suggesting that interdiffusion indeed takes place ($w > \sigma$): an additional 0.6 nm out of the total $w = 1$ nm.

To summarize, *gentle*DB TOF SIMS is a direct technique to obtain chemical information about a sample. It includes elemental, trace impurity distributions as well as isotope distributions in isotopically modulated structures, such as in [33]. While such capabilities are typical for SIMS, in the case of *gentle*DB they are available with greatly enhanced depth resolution. When combined with an analytical MRI model, *gentle*DB high-depth resolution data provide new structural information distinguishing between interdiffusion and native/jig-sawed roughness at buried interfaces in nanolayered materials (as evidenced by XRR measurements). Importantly, *gentle*DB TOF SIMS does not require prior assumptions regarding the sample and does not depend on the sample's optical properties—as opposed to XRR and ellipsometry. It is destructive, but, unlike TEM, does not require sample preparation. Thus, the introduced technique has great potential to become a standard characterization tool to provide essential structural and chemical information for a diverse range of applications in nanotechnology.

Acknowledgments

The authors would like to thank A Yanguas-Gil (ESD, ANL) for valuable discussions. This work was supported under Contract No. DE-AC02-06CH11357 between UChicago Argonne, LLC, and the US Department of Energy (SIMS characterization with *gentle*DB depth profiling, MRI model-based interpretation of experiments) and by NASA through grants NNH08AH76I (hardware for the *gentle*DB sputter depth profiling) and NNH09AM48I (testing and optimization methodology for the *gentle*DB depth profiling including white light profilometry). QP and JWE were supported by 'The Development of Large-Area Fast Photo-detectors' project funded by the US Department of Energy, Office of Science, Office of Basic Energy Sciences and Office of High Energy Physics under Contract DE-AC02-06CH11357. Detailed electron microscopy of ion milled craters was performed at the Electron Microscopy Center for Materials Research at Argonne National Laboratory, a US Department of Energy Office of Science Laboratory, operated under Contract No. DE-AC02-06CH11357 by UChicago Argonne, LLC.

Appendix. The mixing–roughness–information (MRI) model

In concert with [27, 28], conceptually the MRI model relies on solving a differential equation for an ideal flat layer of thickness d, which contains a term determining the ion mixing through a fundamental parameter w, the ion mixing length,

$$\frac{\mathrm{d}c(z)}{\mathrm{d}z} + \frac{1}{w}c(z) = \frac{1}{w}c_{\mathrm{act}}(z+w). \tag{A.1}$$

This equation is solved with simultaneous fulfilment of the boundary conditions

$$c^{\mathrm{up}}|_{z_1-w} = 0, \qquad c^{\mathrm{up}}|_{z_2-w} = c^{\mathrm{down}}|_{z_2-w}, \qquad c_{\mathrm{act}}(z+w)|_{z\geq z_2-w} = 0, \tag{A.2}$$

where $c(z)$ and $c_{\mathrm{act}}(z+w)$ are the apparent (at depth z) and actual (at w deeper than z) concentrations of an element, respectively; z_1 and z_2 are flat boundaries of the layer of thickness d, such that $z_2 - z_1 = d$.

Thus, the solution of equation (A.1) with boundary conditions (A.2) is as follows (represented as a green curve comprised of open circles in figure 2(b)):

$$c(z) = \begin{cases} 1 - \exp\left(-\dfrac{z - z_1 + w}{w}\right), \\ \qquad \text{if } z \in [z_1 - w; z_2 - w] \\ \left(1 - \exp\left(-\dfrac{z_2 - z_1}{w}\right)\right)\exp\left(-\dfrac{z - z_2 + w}{w}\right), \\ \qquad \text{if } z \geq z_2 - w. \end{cases} \tag{A.3}$$

The next steps introduce convolutions of the solution (A.3), due to the ion mixing, with functions describing two other distortion mechanisms which additionally alternate the rectangular depth profile one would expect from the ideal flat layer (represented as the black solid line in figure 2(b)).

The first convolution is due to the roughness (either inherent, or induced, or both), in which the solution (A.3) is convolved with a Gaussian function with RMS roughness σ as the standard deviation (width of the Gaussian bell). The

profile additionally broadens and becomes more symmetric, as illustrated in figure 2(b) (red curve comprised of open squares),

$$C(z) = \frac{1}{\sigma\sqrt{2\cdot\pi}} \int_{-\infty}^{\infty} c(t) \exp\left(-\frac{(z-t)^2}{2\cdot\sigma^2}\right) \mathrm{d}t. \quad (A.4)$$

Practically, it is convenient to use $z \pm n\sigma$ instead of $\pm\infty$ as integration limits, with an error of 30% down to 0.0001% as n ranges from 1 to 5, respectively.

The final profile gets its shape when $C(z)$ undergoes convolution with the $\exp(-x/\lambda)$ function, which takes into account the finite escape depth of the secondary species, λ, or the information depth by the definition of Hofmann [27, 28]. Generally, this final convolution would broaden the red square curve in figure 2(b) even more, but in the case of SIMS it has a negligible contribution in the elemental peak dependence on the depth, $C(z)$, being defined dominantly by the ion mixing and roughness, since the escape depth of secondary ions is 1–2 topmost atomic layers. This second convolution is very important in cases of ion sputter depth profiling in x-ray photoelectron and Auger electron spectroscopies (XPS and AES), where the escape depth is 1–3 nm. Here, the effect of preferential sputtering, which means that in multicomponent materials one of the elements depletes faster/slower than the others under ion bombardment, is not considered. It is known that in the metal-oxide binaries (MgO/ZnO) forming the stack this effect is not present. Otherwise, equation (A.1) would contain one more term on its right-hand side to take this effect into account [27].

References

[1] Hopkins P, Duda J, Petz C and Floro J 2011 *Phys. Rev.* B **84** 035438
[2] Mtsuko D, Avnon A, Lievonen J, Ahlskog M and Menon R 2008 *Nanotechnology* **19** 125304
[3] Wang C, Kohn A, Wang S G and Ward R C C 2011 *J. Phys.: Condens. Matter* **23** 116001
[4] Dash S, Sharma S, Le Breton J, Peiro J, Jaffrès H, George J M, Lemaître A and Jansen R 2011 *Phys. Rev.* B **84** 054410
[5] Bakonyi I and Péter L 2010 *Prog. Mater. Sci.* **55** 107
[6] de Pauli M, Malachias A, Westfahl H, Bettini J, Ramirez A, Huang G S, Mei Y F and Schmidt O G 2011 *J. Appl. Phys.* **109** 063524
[7] Biswas A and Bhattacharyya D 2011 *J. Appl. Phys.* **109** 084311
[8] Jeong H Y, Kim Y I, Lee J Y and Choi S-Y 2010 *Nanotechnology* **21** 115203
[9] Valkovskiy G A, Baidakova M V, Brunkov P N, Konnikov S G, Yagovkina M A and Zadiranov J M 2011 *Phys. Status Solidi* a **208** 2623
[10] Jensen J M, Oelkers A B, Toivola R, Johnson D C, Elam J W and George S M 2002 *Chem. Mater.* **14** 2276
[11] Baena J D, Jelinek L and Marqués R 2005 *New J. Phys.* **7** 166
[12] Monsoriu J A, Depine R A, Martínez-Ricci M L, Silvestre E and Andrés P 2009 *Opt. Lett.* **34** 3172
[13] Chiba D, Akiba N, Matsukura F, Ohno Y and Ohno H 2000 *Appl. Phys. Lett.* **77** 1873
[14] Zhong X Y, Kabius B, Schreiber D K, Eastman J A, Fong D D and Petford-Long A K 2012 *Appl. Phys. Lett.* **100** 101604
[15] Lee D-J, Kim H-M, Kwon J-Y, Choi H, Kim S-H and Kim K-B 2011 *Adv. Funct. Mater.* **21** 448
[16] McKeegan K D, Kallio A P A, Heber V S, Jarzebinski G, Mao P H, Coath C D, Kunihiro T, Wiens R C, Nordholt J E, Moses R W, Reisenfeld D B, Jurewicz A J G and Burnett D S 2011 *Science* **332** 1528
[17] Mrksich M 2008 *ACS Nano* **2** 7
[18] Vickerman J C and Gilmore I S 2009 *Surface Analysis: The Principal Techniques* (Chichester: Wiley)
[19] Putkonen M, Sajavaara T and Niinistö L 2000 *J. Mater. Chem.* **10** 1857
[20] Lujala V, Skarp J, Tammenmaa M and Suntola T 1994 *Appl. Surf. Sci.* **82/83** 34
[21] Elam J W, Sechrist Z A and George S M 2002 *Thin Solid Films* **414** 43
[22] Veryovkin I V, Tripa C E and Pellin M J 2008 *Phys. Proc.* **1** 379
[23] Iltgen K, Bendel C, Benninghoven A and Niehuis E 1997 *J. Vac. Sci. Technol.* A **15** 460
[24] Ormsby T J, Chu D P, Dowsett M G, Cooke G A and Patel S B 1999 *Appl. Surf. Sci.* **144/145** 292
[25] AFM measurements of bottoms of sputtered craters under the same conditions described here, to be published
[26] Baryshev S V, Zinovev A V, Tripa C E, Erck R A and Veryovkin I V 2012 *Appl. Surf. Sci.* **258** 6963
[27] Hofmann S 1992 *J. Vac. Sci. Technol.* B **10** 316
[28] Hofmann S 1994 *Surf. Interface Anal.* **21** 673
[29] Betz G and Wehner G K 1983 *Top. Appl. Phys.* **52** 11
[30] Parratt L 1954 *Phys. Rev.* **95** 359
[31] Asikainen T, Ritala M, Leskelä M, Prohaska T, Friedbacher G and Grasserbauer M 1996 *Appl. Surf. Sci.* **99** 91
[32] Hofmann S 1998 *Rep. Prog. Phys.* **61** 827
[33] Schneider C W, Esposito M, Marozau I, Conder K, Doebeli M, Hu Y, Mallepell M, Wokaun A and Lippert T 2010 *Appl. Phys. Lett.* **97** 192107